



Evaluating YieldTracker Forecasts for Maize in Western Kansas

P. I. Coyne,* R. M. Aiken, S. J. Maas, and F. R. Lamm

ABSTRACT

We seek to predict in-season land productivity to guide irrigation management decisions designed to optimize water utilization in the Ogallala Aquifer region. YieldTracker is a mathematical model that simulates growth and yield of graminoid crops using weather and leaf area index (LAI) as inputs, where LAI can be derived by remote sensing. We tested this model using 3 yr of maize (*Zea mays* L.) yield data from Colby, KS. Four replications of three treatments—rainfed and subsurface drip irrigation (SDI) at 3.8 and 7.6 mm d⁻¹—were compared with simulated yields (36 model runs). Results indicated that YieldTracker has potential as a decision aid for managing irrigated maize, but has insufficient mechanistic complexity to simulate yields of water-stressed maize. YieldTracker projected canopy development well, but LAI does not necessarily correlate with canopy efficiency in capturing solar radiation and converting it to biomass and then partitioning biomass to grain under conditions of limiting soil water. Remotely sensed normalized difference vegetation index (NDVI), a surrogate for LAI, tends to saturate at LAI > 3. Using hyperspectral reflectance data, we found a total chlorophyll vegetation index (TCI) responded nearly linearly to LAI values as high as 6. Similarly, a simple ratio vegetation index, based on a narrow band of wavelengths in the red edge spectral region, responded linearly to increasing LAI. Water band indices (WBI) in the 900 to 970 nm waveband were sensitive to changes in TCI as available soil water decreased. Incorporating TCI and a WBI might improve YieldTracker performance across a range of soil water conditions.

MAAS (1992) demonstrated the utility of combining remotely sensed surrogates for crop canopy development and crop growth models in the release of GRAMI, a mathematical model that uses weather and plant canopy observations to simulate growth and yield of graminoid crops. Maas (1992) noted the basic complementary advantage of this union is that the strengths of one technology can compensate for the weaknesses of the other. However, incorporation of remotely sensed information into models is not trivial.

Ko et al. (2005) described the within-season calibration method of GRAMI that allows the model simulation to fit measured values using an iterative numerical procedure. Based on a comparison between measured and simulated values, model parameters and initial conditions that affect crop growth can be changed. The subsequent model iteration produces a new set of simulated values that minimizes the error between simulated leaf area and values of leaf area obtained from remote sensing. An advantage of this procedure is the capability to use infrequent observations to calibrate

the model, which can be obtained through nondestructive techniques such as remote sensing.

Maas (1988a) described four methods of incorporating remotely sensed information into crop growth models including input, updating, reinitialization, and reparameterization. Input is the simplest technique and involves using remotely sensed observations to evaluate model driving variables. Updating involves replacing simulated values of model state variables with values determined from remotely sensed data, thereby providing a new starting point within the growing season each time a simulated value is replaced. Reinitialization and reparameterization involve using an iterative numerical technique to manipulate model initial conditions or parameters so that the resulting simulation fits remotely sensed observations.

In reinitialization and reparameterization, the remotely sensed data are not used directly in computing crop growth, but are used to guide the manipulation of selected model initial conditions or parameters that affect modeled growth. The resulting growth simulation passes through the observed values in the manner of a best fit, such that the effects of random errors in the observations cancel (Maas, 1988a). An advantage of this approach is that even a single observation can significantly improve model performance (Maas, 1988b) enabling the model to simulate much of the detail observed by frequent field observations of crop growth.

P.I. Coyne, Agricultural Research Center, Kansas State Univ., Hays, KS 67601; R.M. Aiken and F.R. Lamm, Northwest Research-Extension Center, Kansas State Univ., Colby, KS 67701; and S.J. Maas, Dep. of Plant and Soil Science, Texas Tech Univ., Lubbock, TX 79409. Contribution no. 08-338-J from the Kansas Agric. Exp. Stn. Received 1 May 2008. *Corresponding author (coyne@ksu.edu).

Published in *Agron. J.* 101:671–680 (2009).
doi:10.2134/agronj2008.0146

Copyright © 2009 by the American Society of Agronomy, 677 South Segoe Road, Madison, WI 53711. All rights reserved. No part of this periodical may be reproduced or transmitted in any form or by any means, electronic or mechanical, including photocopying, recording, or any information storage and retrieval system, without permission in writing from the publisher.



Abbreviations: ASW, available soil water; ASWI, available soil water index; dIR, first derivative of reflectance; HI, harvest index; LAI, leaf area index; NDVI, normalized difference vegetation index; NIR, near infrared; R, reflectance; RMSE, root mean square error; RUE, radiation use efficiency; SDI, subsurface drip irrigation; SLA, specific leaf area; SR, simple ratio; TCI, total chlorophyll index; VI, vegetation index; VBA, Visual Basic for Applications; WBI, water band index; WBDInt, integral of the water band first derivative; YPF, yield partitioning factor.

YieldTracker, a mathematical crop growth model of the form described by Maas (1993), uses remotely sensed data for within-season calibration of crop growth simulations. YieldTracker evolved from GRAMI to serve as the core model of a project designed to provide farmers within-season predictions of crop yield in individual fields over the Internet (Maas et al., 2003). These predictions are intended to support real-time management decisions such as irrigation water applications. YieldTracker depends on regional weather observations and satellite remote sensing to develop probabilistic predictions of crop yield during the growing season. Versions of the YieldTracker model applicable to the three major warm-season crops in the region of interest are being used including maize (*Zea mays* L.), cotton (*Gossypium hirsutum* L.), and sorghum [*Sorghum bicolor* (L.) Moench].

Estimates of plant canopy leaf area index (LAI) used for model calibration are commonly derived from vegetation indices such as the normalized difference vegetation index (NDVI) extracted from Landsat TM imagery acquired during the growing season. A deficiency in this approach is the limited sensitivity of NDVI to dense canopies (e.g., LAI > 3) as demonstrated by Myneni et al. (1997) for six structural types of land cover including grasses and cereal crops.

Knowledge of in-season land productivity can guide management needed to optimize water utilization. Satellite images can quantify crop canopy formation and yield potential of individual fields in large, multi-county regions. Dynamic quantification of land productivity can support analysis of risks associated with water use as well as demonstrating the value of information analysis. Much of western Kansas overlies the Ogallala Aquifer, which is being mined by pumping. Extending the life of this resource by prudent use seems paramount to sustaining the local and state economies. Therefore, our research objectives were to evaluate the accuracy of maize yield forecasts from the YieldTracker model for western Kansas conditions over a range of soil water conditions and to investigate alternative vegetative indices to NDVI that respond to plant water status and high values of LAI.

MATERIALS AND METHODS

YieldTracker Code

An early version of YieldTracker coded in DOS FORTRAN—and parameterized for maize growing in the High Plains of Texas—was ported to Visual Basic for Applications (VBA) to run under Microsoft Access (Microsoft Corporation, Redmond, WA). The crop growth and partitioning algorithms and the numerical solution were as described for GRAMI by Maas (1992). A graphical user interface was added to provide flexibility for managing input datasets, manipulating run conditions, and exploring parameter sensitivity. A graphics module coded in MatLab (The Mathworks, Natick, MA) was also developed to visually display selected model input and output datasets.

Model Validation Dataset

Maize production data from a subsurface drip irrigation study at the Kansas State University Northwest Research-Extension Center in Colby were obtained for the years 2002–2004. End-of-season grain yield and in-season development of LAI data were available from four replications

of three treatments—(i) no in-season irrigation (rainfed), (ii) limited irrigation (3.8 mm d⁻¹), and (iii) full irrigation (7.6 mm d⁻¹)—to serve as validation datasets. Subsurface drip irrigation was scheduled daily according to the determined need from a weather-based water budget, but was intentionally limited to the maximum irrigation system capacities of 3.8 mm d⁻¹ (limited irrigation treatment) and 7.6 mm d⁻¹ (full irrigation treatment) to simulate an irrigation application rate constrained by hydrologic groundwater characteristics. The limited irrigation treatment received a total of 331, 320, and 271 mm of irrigation water in 2002, 2003, and 2004, respectively. Corresponding values for the full irrigation treatment were 518, 465, and 373 mm. Target plant population was 88,920 plants ha⁻¹.

To eliminate one source of variability for this validation exercise, field measurements of the seasonal progression of LAI were used to adjust simulated canopy development rather than estimating LAI from remotely sensed NDVI as might normally be the case. Leaf area of the maize canopy was determined by light transmission using a LI-COR 2000 Plant Canopy Analyzer (LI-COR Biosciences, Lincoln, NE). Downwelling diffuse radiation above the canopy was quantified for each of five hemispherical ranges of angles, providing reference radiation. Diffuse radiation transmitted through the canopy, in the same ranges of angles, was detected using three sets of four stratified samples beneath the crop canopy. Canopy characteristics, including LAI, were derived from an application of the Beer-Lambert Law (Welles and Norman, 1991), following the manufacturer's instructions.

Local weather data (average daily temperature, global short-wave irradiance) were used as model driving variables. Annual precipitation was 362, 369, and 513 mm for 2002, 2003, and 2004, respectively, compared with the 30-yr mean of 512 mm. The years 2002 and 2003 were considered to represent severe drought (both hot and dry), while 2004 was near normal conditions. Precipitation during the cropping season was 269, 232, and 311 mm for 2002 to 2004, respectively, as compared with the normal of 305 mm. Calculated evapotranspiration, for the 120-d period 15 May through 11 September, was much above the long-term normal (584 mm) in 2002 and 2003 (703 and 659 mm, respectively) and near normal in 2004 (573 mm). Hot and dry conditions during 2003 were associated with increased spider mite (*Oligonychus pratensis* Banks and *Tetranychus urticae* Koch) pressure, which was not fully controlled by two insecticide treatments applied on 20 July and 4 Aug. 2003.

Simulation Runs and Statistical Analysis: 2006

Individual model simulation runs were conducted for each of the 36 yr-treatment-replication combinations. The simulated yields were compared to observed values using standard statistical analysis of variance and the LSD multiple range test for mean separation (Statistix 9, Analytical Software, Tallahassee, FL) to evaluate model performance. The sources of variation for the general linear model were block, year, treatment, block × treatment, and year × treatment.

Field Procedures: 2007

Because remote sensing of canopy development was ultimately a goal, we measured hyperspectral reflectance signatures

above maize canopies during the 2007 growing season. These data were used to search for vegetation indices that were more sensitive to changes in LAI and plant water status than NDVI. Field observations of maize canopy development spanned a range of soil water conditions and stages of development from mid-vegetative growth through canopy senescence. Annual precipitation recorded in 2007 was 466 mm. Replicated (3×) plots of three field studies—including rainfed, limited irrigation, and full irrigation treatments—provided the expected range of water status and maize canopy conditions typical of the central U.S. High Plains. A rainfed cropping sequence study represented severe water deficit conditions. Four experimental treatments included maize grown in a wheat (*Triticum aestivum* L.)-maize-fallow crop sequence or in continuous cropping sequences of wheat-maize-oilseed. Oil seeds treatments included spring canola (*Brassica napus* L.), soybean [*Glycine max* (L.) Merr.], or sunflower (*Helianthus annuus* L.). Two treatments of a subsurface drip irrigation study represented early season stress, where water deficits formed in an initially full soil water profile with full seasonal irrigation commencing either 1 wk before silking or at silking. Six treatment combinations of a tillage and sprinkler irrigation capacity study represented mid- and late-season stress as well as water sufficiency. Irrigation was scheduled with a weather-based water budget, but was limited to the two sprinkler irrigation system capacities of 25 mm every 4 or 8 d (equivalent to 6.4 or 3.2 mm d⁻¹). This translates into typical seasonal irrigation quantities of 375 to 500 mm and 200 to 300 mm, respectively. Three tillage treatments (no-till, strip-till or conventional till) were included in the study. Field studies were managed to minimize pest and nutrient constraints to crop productivity.

Canopy hyperspectral reflectance and LAI were measured for each experimental treatment throughout the growing season. Canopy observations commenced in mid-June, 5 wk after planting, and continued at biweekly intervals through mid-September. Hyperspectral solar reflectance was measured using a GER 1500 Spectroradiometer (Spectra Vista Corporation, New York, NY). Downwelling solar radiation, reflected by a Spectralon thermoplastic resin, provided a measure of reference radiation (300–1085 nm wavelengths, 512 bands). Upwelling shortwave radiation was transmitted to the radiometer by a fiber-optic cable, oriented vertically with respect to canopy at an elevation of 3 m above the soil surface. Upwelling and downwelling radiation spectra were linearly interpolated to gain 1 nm resolution. Reflectance was calculated as the ratio of upwelling to downwelling radiation at 1 nm intervals. Canopy reflectance and LAI transmittance observations were typically completed on the same date for a given set of plots.

Vegetation Index Calculations

Hyperspectral reflectance (*R*) scans from 2007 were used to calculate four vegetation indices. Normalized difference vegetation index (NDVI) was calculated using Landsat TM and ETM+ red and near infrared (NIR) band equivalents [NDVI = ($R_{750-900} - R_{630-690}$) / ($R_{750-900} + R_{630-690}$)]. A total chlorophyll index [TCI = ($R_{750-800} / R_{695-740}$) - 1] was computed using the method of Gitelson et al. (2003). A water band index [WBI = (R_{900} / R_{970})] was based on Peñuelas et al. (1993). In

addition, the reflectance first derivative was integrated over the wave band 900 to 970 nm (WBd1Int).

Average reflectance across a specific wave band was used in these calculations.

Sensitivity of water band indices to changes in TCI as a function of available soil water was examined. Soil water was measured by neutron attenuation (Campbell Pacific Nuclear, Hydroprobe Model 503 DR). Weekly to biweekly soil water measurements were made in 0.3-m increments to 2.4-m depth. All data were taken near the center of each plot. These data were utilized to examine treatment differences in soil water conditions both spatially (e.g., vertical differences) and temporally (e.g., differences caused by timing of irrigation in relation to evaporative conditions as affected by residue and crop growth stage). Available soil water was expressed on a volumetric basis.

The 2007 hyperspectra were also analyzed to find optimal wavelength pairs that maximized the correlation between a vegetation index (VI) and LAI. Adapting the methods of Mutanga and Skidmore (2004), we calculated vegetation indices for all possible wavelength pairs (186,355) between the limits 390 to 1000 nm for 143 hyperspectra collected from plots representing diverse environments throughout the 2007 growing season. Corresponding LAI was measured in each plot. Correlation coefficients for all of the 143 VI–LAI datasets were computed and used to sort the wavelength pairs (λ_1 , λ_2) from high to low in search of those pairs that best linearized the VI–LAI relationship. Vegetation index was based on the general equations for either NDVI [$(\lambda_2 - \lambda_1) / (\lambda_2 + \lambda_1)$] or SR [λ_2 / λ_1].

RESULTS AND DISCUSSION

YieldTracker Performance

The analysis of variance for observed minus YieldTracker simulated yields, plus the model goodness of fit for seasonal development of LAI, indicated a significant year × treatment interaction. Therefore, only the year × treatment means are discussed here (Table 1). Yields from the rainfed treatment were consistently overpredicted, whereas the yields from the irrigated treatments were consistently underpredicted across years. Yields from the rainfed treatment were significantly lower than

Table 1. All-pairwise year × treatment mean comparisons of YieldTracker yield simulations and LAI goodness-of-fit. Means followed by a unique letter are significantly different.

Specific interaction		Yield	Observed – simulated	Goodness-of-fit
Year	Treatment			
		kg ha ⁻¹		%
2002	rainfed	4,258f	-6,185e	85.5d
2002	limited irrigation	13,932cd	587c	88.3bcd
2002	full irrigation	16,556b	2,582a	87.9cd
2003	rainfed	2,076g	-9,719f	93.4a
2003	limited irrigation	13,152d	821bc	93.1a
2003	full irrigation	14,783c	2,680a	93.9a
2004	rainfed	11,341e	-2,802d	87.0cd
2004	limited irrigation	17,681a	2,630a	92.0ab
2004	full irrigation	17,150ab	1,918ab	90.8abc
	Standard error	447	527	1.8
	Critical value	939	1,108	3.9
	t-value for $\alpha = 0.05$; df = 18	2.101		Error term: block × year × treatment

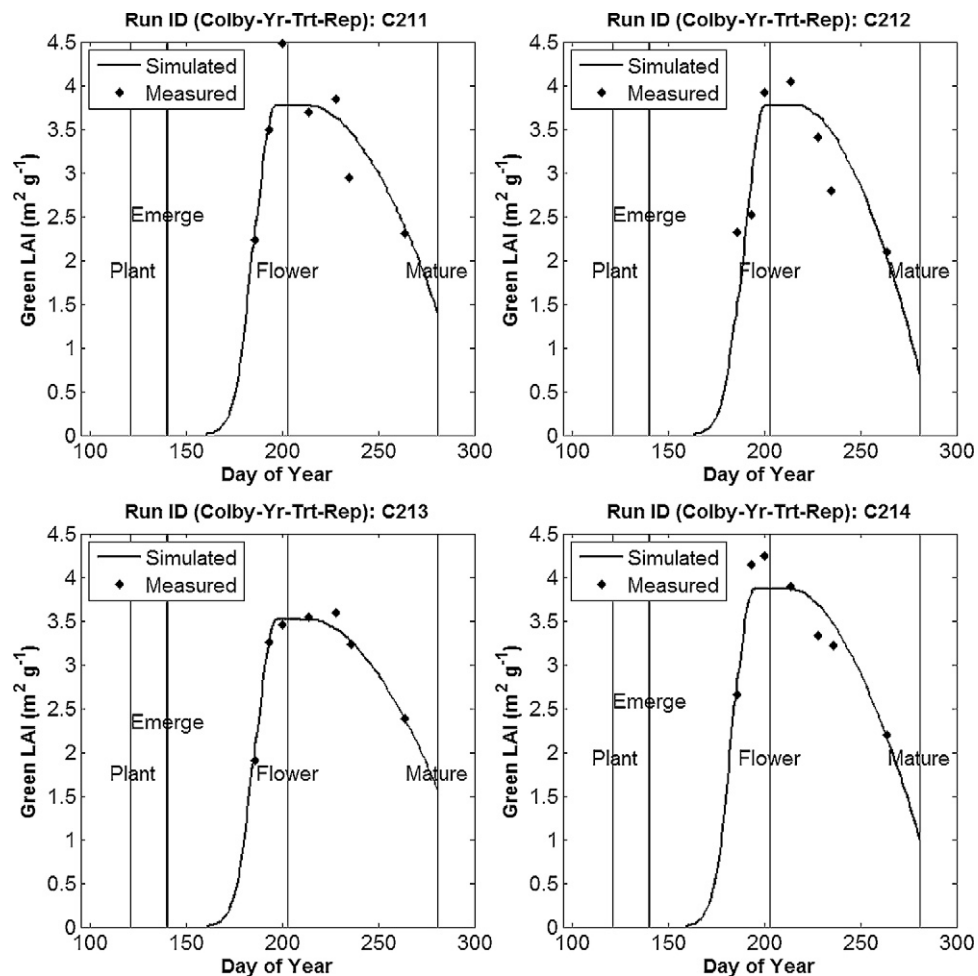


Fig. 1. YieldTracker projections of canopy development (leaf area index, LAI) for the rainfed treatment in 2002. Four replications are shown.

the irrigated treatments in all 3 yr. In addition, yields within the rainfed treatment were different in all 3 yr. Precipitation in 2002 and 2003 was 88 and 76% of the long-term mean, respectively. This was reflected in yields, which were significantly higher in the full irrigation treatment than in the limited irrigation treatment. In 2004, precipitation matched the long-term mean and full irrigation had no yield advantage compared with limited irrigation. Accurate in-season prediction of yields could possibly eliminate late season irrigations in situations similar to 2004, thereby saving water and reducing input costs.

The relatively high values (Table 1) for the LAI goodness-of-fit (85–94%) suggest that the significant differences between observed and simulated yields were not linked to canopy development simulations. An example of the seasonal course of observed and simulated green LAI is presented in Fig. 1 for all four replications of the rainfed treatment in 2002, which had the lowest average goodness-of-fit (85%, Table 1) among treatments and years. The model was able to track LAI reasonably well. However, discrepancies among observed vs. simulated yields were significant. This likely resulted from incorrect parameterization or insufficient mechanistic complexity in model algorithms that convert solar radiation to biomass or allocate biomass to grain rather than those that simulate canopy development.

Sensitivity analyses revealed the effect of selected parameter values on simulated grain yield. We conducted these analyses

by changing a model parameter iteratively within an interval bracketing the default setting, while holding other parameters constant. Two extreme runs (Fig. 2) showed that the primary influence of specific leaf area (SLA = ratio of unit leaf area to unit leaf mass) was at very low values. In the limited irrigation treatment, where YieldTracker performed best, SLA could be increased (less costly leaves) to raise simulated grain yield to the observed. However, in the rainfed treatment, SLA would have to be reduced to unrealistic levels (very costly leaves) to force simulated yield to match observed yield. Similarly, the default yield partitioning factor (YPF) value (0.75) produced a near perfect match for limited irrigation. However, a value of about 0.1 was required to make simulated mimic observed yield in the rainfed treatment.

Overall, simulated yields under limited and full irrigation were slightly underpredicted, while simulated yields for the rainfed condition were generally severely overpredicted (Fig. 3). The individual data points, plus the standard deviation error bars, show that scatter or variability within treatments, especially rainfed, was attenuated by the model compared with observed yields.

The appeal of YieldTracker is its unique numerical solution requiring the user to input, in addition to temperature and radiation data, only one or more green LAI observations. Such LAI values can be obtained by methods of destructive sampling or remote sensing. Effects of water stress must be accounted for

by changes in LAI. Earl and Davis (2003) have published conclusive evidence that drought stress reduces yield of maize and other grain crops by reducing radiation-use efficiency (RUE), harvest index (HI), and canopy absorption of incident light in that order of impact. To make this model maximally useful for water management decisions in western Kansas, the algorithm needs to account for these effects.

Because of the utility of YieldTracker—related to its simplicity and minimal driving variable data requirement—the possibility of modification to improve its performance seems worthwhile. Remote sensing offers potential for straightforward, wide-area quantification of the seasonal course of crop canopy development. YieldTracker projects the course of green LAI quite well. Yet the traditional use of NDVI as a surrogate for LAI suffers in crops like maize, where LAI values typically exceed 3 and are often as high as 6 or more. The NDVI saturates asymptotically as LAI increases above 3. In addition to the need for improved tracking of high LAI, some indicator of canopy functionality or efficiency is required to modify the simulated biomass production and allocation to grain as plant water status responds to decreasing available soil water. Earl and Davis (2003) demonstrated the effects of water deficits on RUE, HI, and light absorption under field conditions. Detecting water deficit conditions and quantifying effects on canopy function could improve YieldTracker performance under water-limiting conditions.

Hyperspectral Reflectance Analyses

To address the issue of remote sensing of canopy development, we used hyperspectral reflectance signatures from maize growing in a wide range of available soil water conditions and found vegetation indices that were more sensitive to changes in LAI and plant water status. The NDVI showed the expected curvilinear response to increasing LAI, while TCI—consistent with the findings of Gitelson et al. (2003)—was nearly linear up to LAI = 6, and the WBI response was intermediate between these two indices (Fig. 4, Table 2). The R^2 values for the linear and exponential models of TCI were almost equal, indicating the utility of this index for high LAI crops like maize as reported by Gitelson et al. (2003).

Available soil water (ASW) ranged from 44 to 466 mm in a 2.4 m profile. An ASW index (ASWI = 1–5) was created where 1 = 44 to 100, 2 = 100 to 200, 3 = 200 to 300, 4 = 300

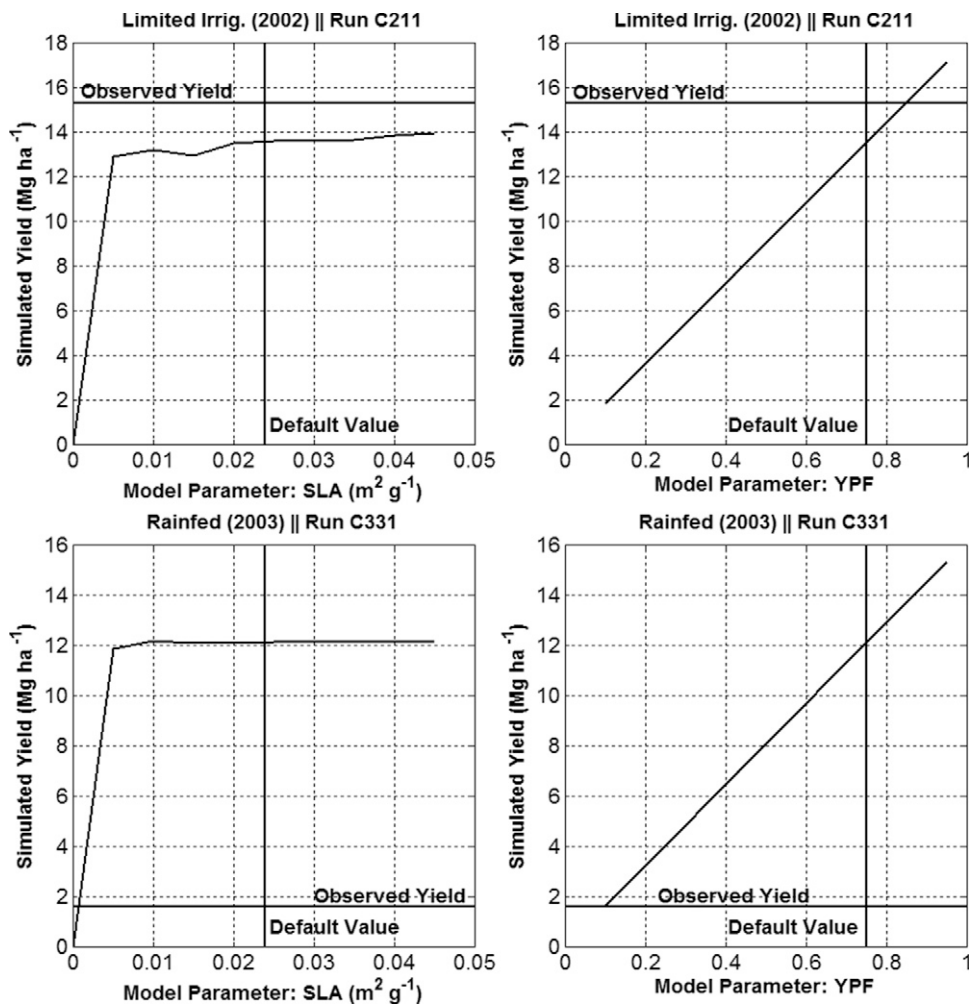


Fig. 2. Sensitivity of YieldTracker yield predictions to specific leaf area (SLA) and yield partitioning factor (YPF) for the limited irrigation treatment in 2002 (top) and the rainfed treatment in 2003 (bottom).

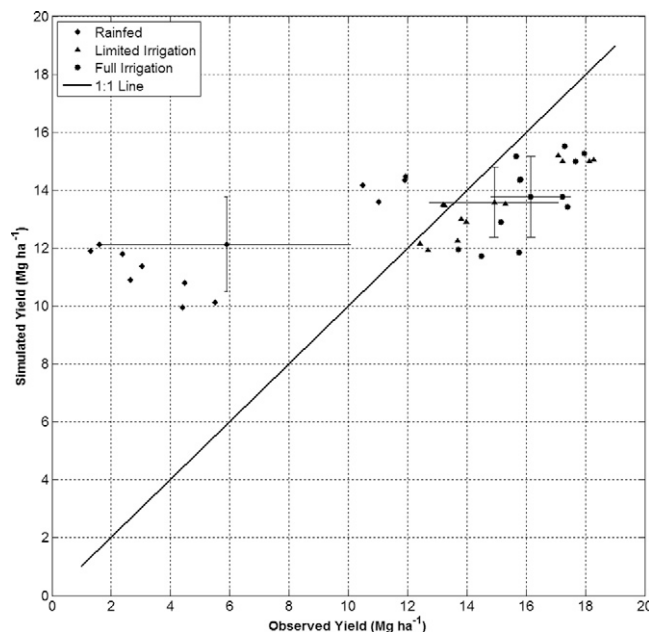


Fig. 3. YieldTracker simulated mean yields across years, treatments, and replications vs. observed mean yields. Error bars are means \pm standard deviation.

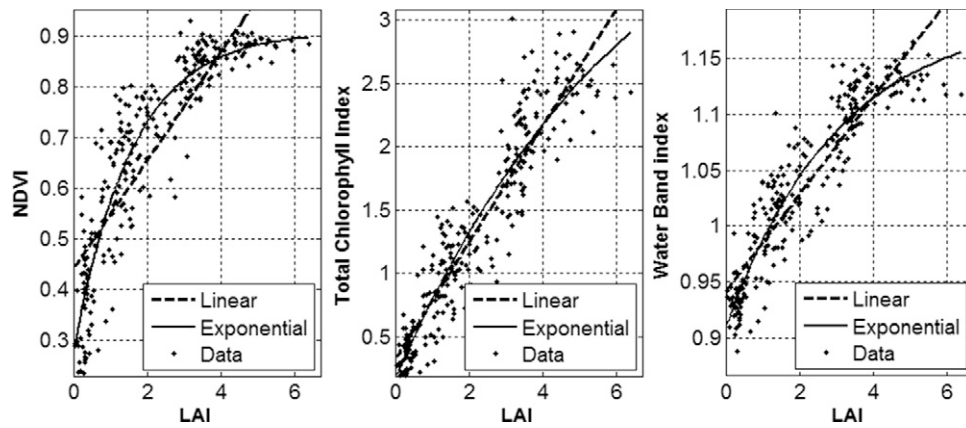


Fig. 4. Sensitivity of normalized difference vegetation index (NDVI), total chlorophyll index (TCI), and water band index (WBI) to leaf area index (LAI).

to 400, and 5 = 400 to 466. The sensitivity of water band indices to changes in TCI was determined using data associated with each ASWI.

Water band indices, WBI and WbdlInt, responded in a near-linear manner to increasing TCI (Fig. 5) as expected since both indices are spectrally derived and correlated with LAI. Within an ASWI, the sensitivity of the WB indices to increasing TCI decreased as ASW increased. Similar results have been reported by Gamon et al. (1999). This suggests that these indices have potential to modulate radiation capture and conversion efficiency as well as dry matter partitioning algorithms in YieldTracker. It is possible that useful information for water deficit conditions will come from water balance algorithms that utilize crop coefficients derived from remote sensing of surface temperatures and potential evaporation to calculate crop water use (Bastiaanssen et al., 1998).

Similar to the results of Mutanga and Skidmore (2004), the VI–LAI relationships, based on all possible wavelength pairs, were most linear in the red edge spectral region (e.g., 720–760 nm). This is not surprising because the sensitivity of reflectance in the red edge band to changes in wavelength is higher than for any other green leaf spectral feature in the visible and NIR

(Elvidge and Chen, 1995). Red edge reflectance is particularly responsive to changes in canopy biomass (LAI) and leaf chlorophyll content as a result of contrasting high adsorption by chlorophyll in the red and corresponding high reflectivity arising from cell wall scattering in the NIR (reviewed by Mutanga and Skidmore, 2004). As a result, optimal wavelength pairs for the top 10 and top 50 correlation coefficients were separated by only a few nm and confined to the bands of 748 to 755 and 744 to 756 nm, respectively. Mutanga and Skidmore (2004) reported the wavelength pairs for the 10 highest NDVI–biomass correlation coefficients ranged from 716 to 762 nm and the highest *r*-value (0.886) occurred at wavelengths of 746 and 755 nm.

An example hyperspectral reflectance scan at full crop canopy development is reproduced at two scales in Fig. 6. The first derivative (d1R) of reflectance is also plotted. The optimal wavelength pairs occurred within the longer wavelength region of the red edge transition including wavelengths greater than the point of maximum slope as shown by d1R. Among all 143 scans, there was an occasional local d1R minimum (22 out of 143) within the 744 to 756 nm band. A local d1R maximum was generally observed at or just beyond the 756 nm limit, but within this band, the maximum d1R always corresponded to the 744 nm limit.

Still in search of a linear prediction equation, we computed NDVI and SR for three different wavelength pairs. The first set ($\lambda_1 = 748, \lambda_2 = 755$ nm) represents the waveband limits that gave the 10 highest VI–LAI correlation coefficients, where λ_1 and λ_2 ranged between 390 and 1000 nm at 1-nm intervals. The second set ($\lambda_1 = 700, \lambda_2 = 774$ nm) represents the wavelength pair that gave the highest VI–LAI correlation coefficient when λ_1 was constrained to 600 to 700 nm and λ_2 was constrained to 700 to 900 nm. Finally, the third set ($\lambda_1 = 660, \lambda_2 = 825$ nm) represents the midpoints of the Landsat TM and ETM+ red and NIR bands, respectively. Results for NDVI–LAI are plotted in Fig. 7. Results for SR–LAI are plotted in Fig. 8. Using the narrow band of wavelengths (Fig. 7, left), even the NDVI–LAI relationship approached linearity ($R^2 = 0.90$), but constraining the choice of wavelength pairs (Fig. 7, center), or using Landsat wavelengths (Fig. 7, right), did not provide an usable VI. However, the superiority of the SR equation, compared with the NDVI equation, is shown in the companion SR–LAI plots (Fig. 8). Although the narrowest band (Fig. 8, left) was still superior to

Table 2. Linear and exponential regression models for vegetation index (y) vs. leaf area index (x), where vegetation index is normalized difference vegetation index (NDVI), total chlorophyll index (TCI), or water band index (WBI). Both linear ($y = a + bx$) and exponential [$y = a + (b - a) \times \exp(-cx)$] models were fit.

Model	Parameter	NDVI	TCI	WBI
Linear	R^2	0.736	0.866	0.831
	a	0.440	0.318	0.941
	b	0.107	0.463	0.043
Exponential	R^2	0.854	0.877	0.877
	a	0.910	4.634	1.190
	b	0.272	0.172	0.909
	c	0.633	0.149	0.330
Index	<u>Equation</u>			
NDVI	$(R_{750-900} - R_{630-690}) / (R_{750-900} + R_{630-690})$			
TCI	$(R_{750-900} / R_{695-740}) - 1$			
WBI	R_{900} / R_{970}			

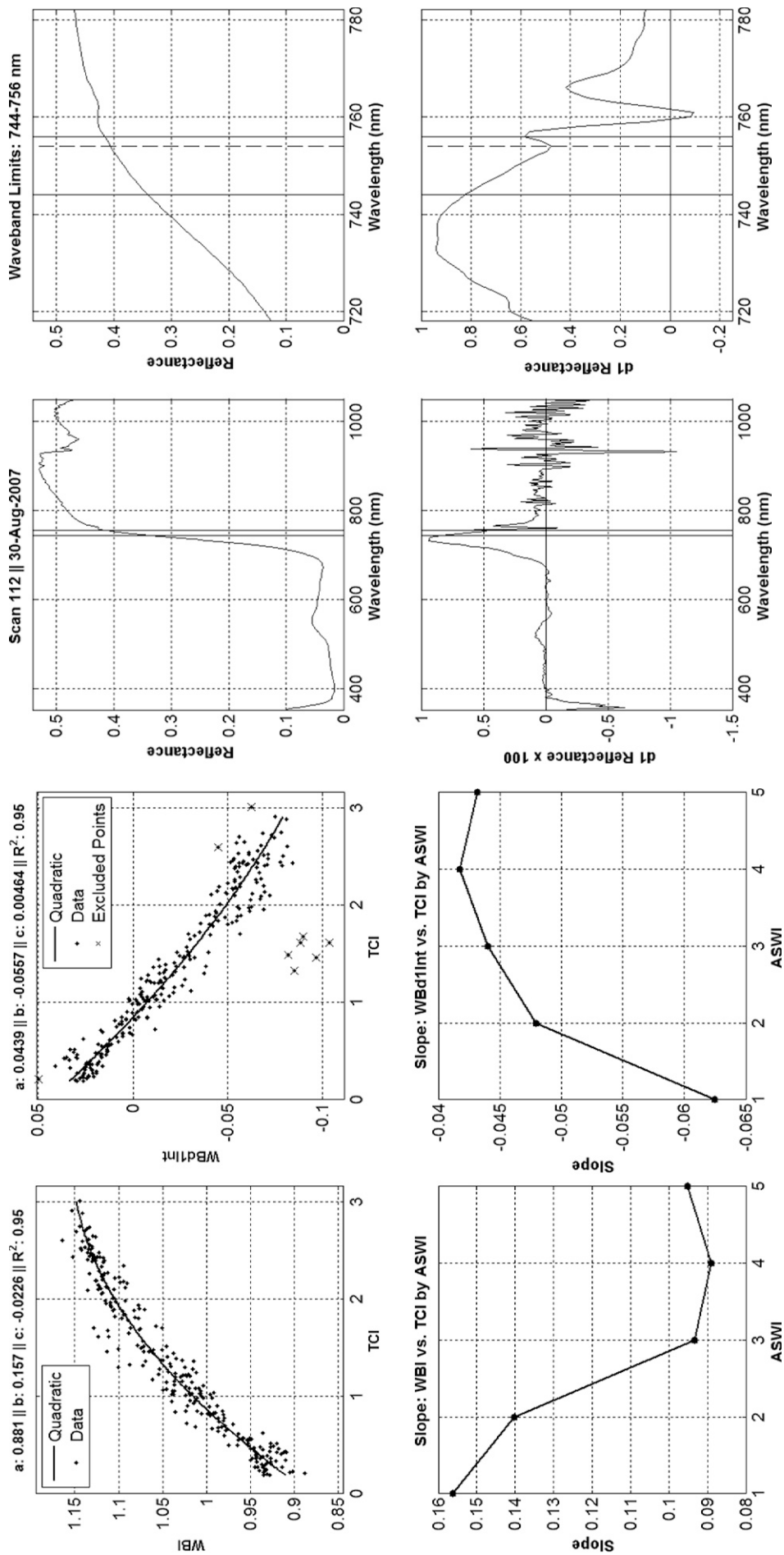


Fig. 5. Regression of water band index (WBI = R_{900}/R_{970}) and the integral of the first derivative of reflectance (WBdInt) in the water band (900–970 nm) on total chlorophyll index or TCI (top) and sensitivity of slope to available soil water index or ASWI (bottom). The coefficients (a , b , c , R^2) are for the equation $y = a + bx + cx^2$.

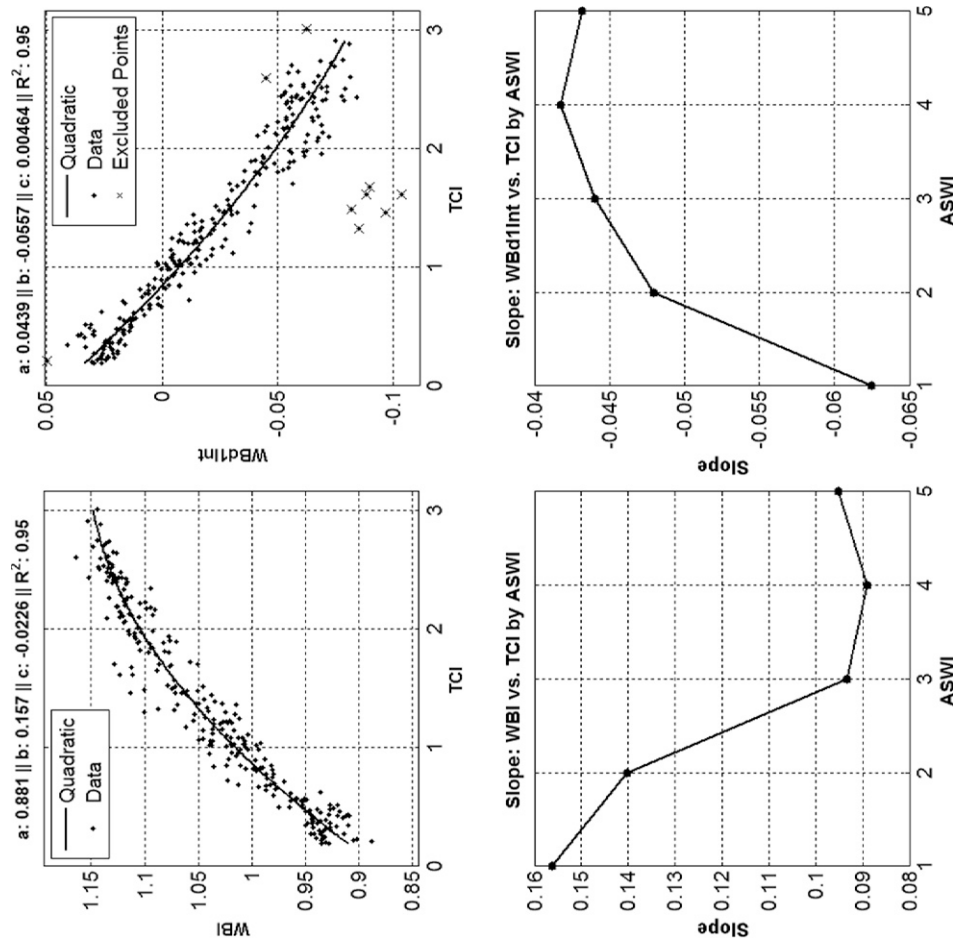


Fig. 6. Example hyperspectral scan for 350 to 1050 nm (left) and the same scan zoomed to the red edge spectral region (right). Reflectance and its first derivative (dI) are plotted on the ordinates. The solid vertical lines mark the waveband (744–756 nm) containing the wavelength pairs that gave the 50 highest (out of 186,355) VI–LAI correlation coefficients, where VI is either normalized difference vegetation index (NDVI) or simple ratio (SR) and LAI is leaf area index. The dashed vertical line marks the location of a local minimum for the reflectance first derivative.

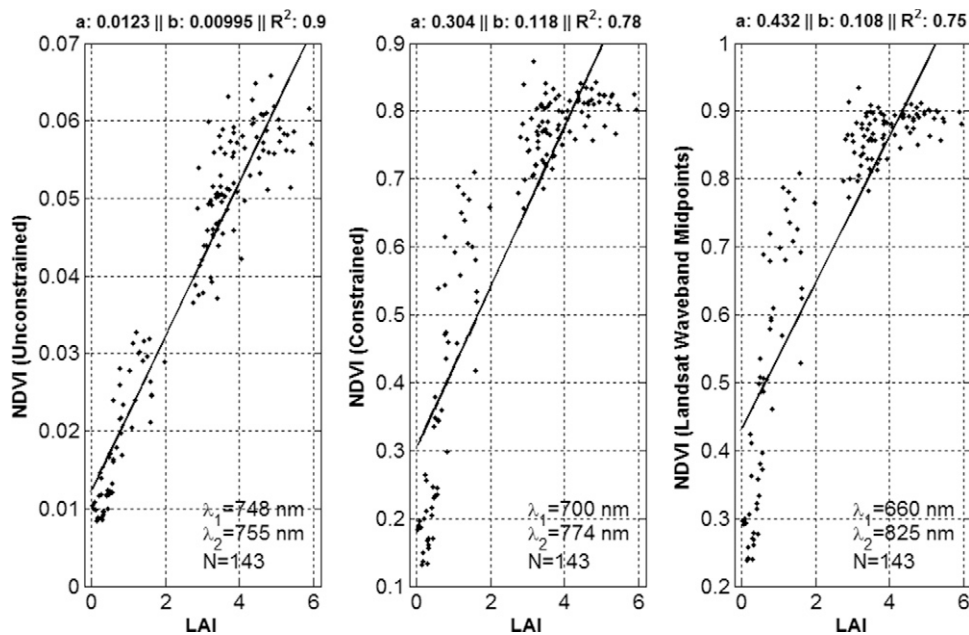


Fig. 7. Normalized difference vegetation index (NDVI) response to increasing leaf area index (LAI) calculated using the wavelength pairs shown. The unconstrained (left) wavelength pair represents the extremes that gave the 10 highest (out of 186,355) NDVI–LAI correlation coefficients, where λ_1 and λ_2 ranged between 390 and 1000 nm at 1-nm intervals. The constrained (center) wavelength pair, where λ_1 was allowed to vary between 600 and 700 nm and λ_2 between 700 and 900 nm, gave the highest NDVI–LAI correlation coefficient. The Landsat (right) wavelength pair represents the midpoints of the red and NIR bands used by the Thematic Mapper and Enhanced Thematic Mapper+ sensors. The coefficients (a , b , R^2) are for the equation $y = a + bx$.

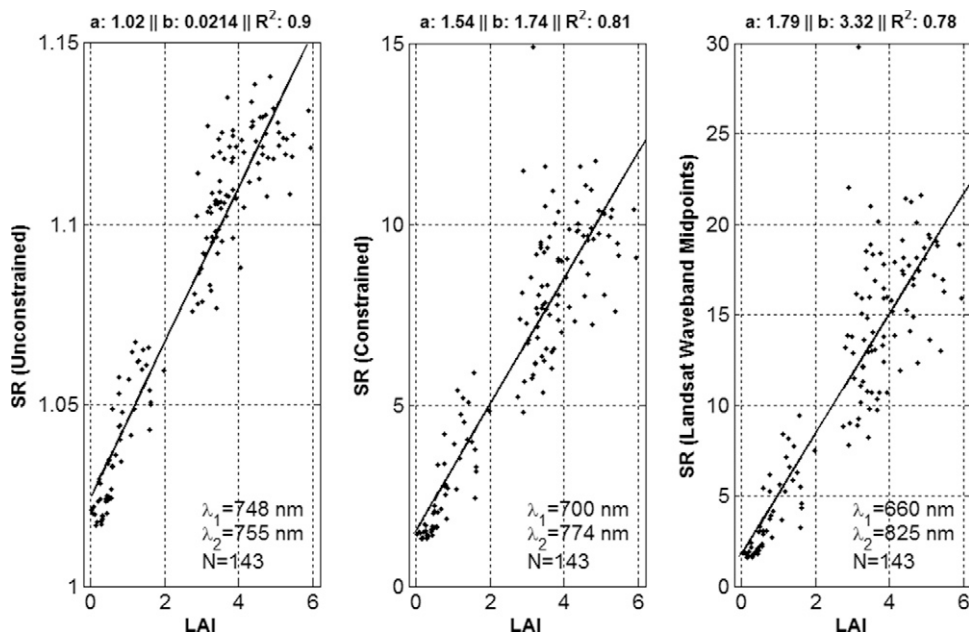


Fig. 8. Simple ratio (SR) response to increasing leaf area index (LAI) calculated using the wavelength pairs shown. The unconstrained (left) wavelength pair represents the extremes that gave the 10 highest (out of 186,355) SR–LAI correlation coefficients, where λ_1 and λ_2 ranged between 390 and 1000 nm at 1-nm intervals. The constrained (center) wavelength pair, where λ_1 was allowed to vary between 600 and 700 nm and λ_2 between 700 and 900 nm, gave the highest SR–LAI correlation coefficient. The Landsat (right) wavelength pair represents the midpoints of the red and NIR bands used by the Thematic Mapper and Enhanced Thematic Mapper+ sensors. The coefficients (a , b , R^2) are for the equation $y = a + bx$.

the other two combinations tested, the SR equation more nearly linearized the relationship compared to NDVI. Serrano et al. (2000) also reported a curvilinear relationship for NDVI–LAI in wheat with LAI values as high as 8, but a linear relationship

for SR–LAI. Their selected wavelengths for both NDVI and SR were in the red (680 nm) and NIR (900 nm).

Using the linear equation for SR–LAI (Fig. 8, left), we computed predicted LAI and compared it to measured LAI for

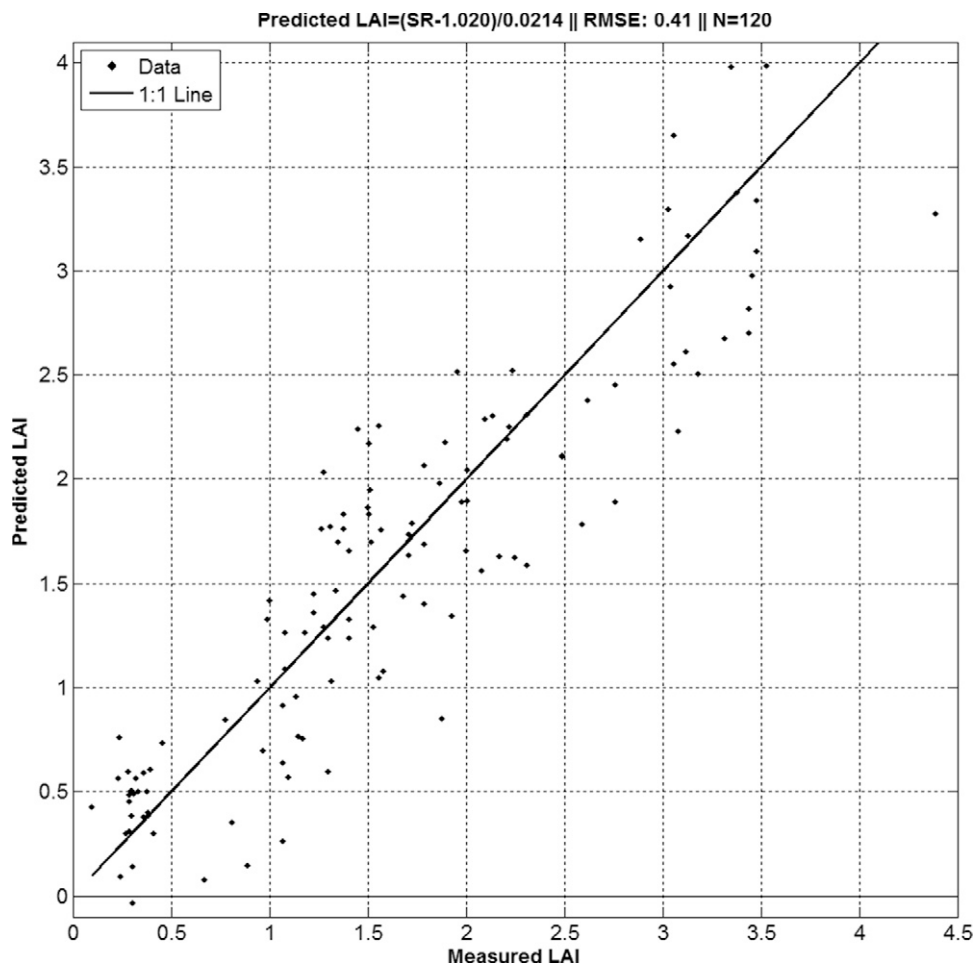


Fig. 9. Predicted leaf area index (LAI)—based on simple ratio ($SR = \lambda_2/\lambda_1$), where $\lambda_1 = 748$ nm and $\lambda_2 = 755$ nm—vs. measured LAI. These wavelengths are the extremes of a band that gave the 10 highest (out of 186,355) SR–LAI correlation coefficients, where λ_1 and λ_2 ranged between 390 and 1000 nm at 1-nm intervals. Predicted LAI was calculated by inverting the unconstrained linear equation from Fig. 8 (left) as shown in header above. Measured LAI is a validation dataset completely separate from the dataset used to calibrate the prediction equation.

a validation dataset that was different from the calibration dataset used in Fig. 8. Simple ratio (λ_2/λ_1 where $\lambda_1 = 748$ nm and $\lambda_2 = 755$ nm) was based on reflectance at the extremes of the spectral band that gave the 10 highest SR–LAI correlation coefficients with the calibration dataset. The calibration dataset represented maize grown under near optimal soil water conditions season long with a maximum LAI value > 6 . The validation dataset represented 120 hyperspectra from maize grown under rainfed or early season water deficit conditions (described in Field Procedures: 2007) as reflected in maximum LAI values < 4.5 . The root mean square (RSME) for the predicted–measured relationship (Fig. 9) was less than 0.5 LAI units, indicating the utility of the red edge spectral region for linearizing vegetation index surrogates for LAI and canopy development.

Thus, our results demonstrate that hyperspectral sensors can provide remotely sensed information that is adequate for simulating crop canopy development by YieldTracker—even in crops like maize, where LAI may exceed 6—provided appropriate vegetation indices and wavelengths are selected. Landsat TM and ETM+ sensors cannot provide the needed resolution, but scanners such as the Compact

Airborne Spectrographic Imager (CASI) from ITRES Research Limited in Canada that can detect 288 wavelength bands between 400 and 1000 nm, may provide the needed resolution for wide area coverage.

What is lacking in YieldTracker is sufficient mechanistic complexity to account for water stress effects on photosynthesis and C partitioning. Sinclair (1991) reported a simple analytical model of radiation capture and use-efficiency for a crop canopy. The model requires leaf area index, daily weighted mean radiation angle, shadow projection coefficient, radiation intensity, leaf quantum efficiency, and biomass conversion efficiency. Radiation capture by sun and shade fractions of the canopy drives simulation of total C assimilation, using a nonrectangular hyperbola to quantify light-limiting effects on photosynthesis. Biomass accumulation assumes constant conversion efficiency, considering respiration effects. This simplified model utilizes a mechanistic conception of radiation capture and biomass accumulation to calculate use-efficiency. As such, it is suitable to quantify effects of incomplete canopy and variable radiation levels on biomass accumulation under water and nutrient sufficiency.

Like YieldTracker, this Sinclair (1991) model does not consider water deficit effects. However, its incorporation of additional physiological detail may make it a better starting point for adding water stress effects—to achieve the objective of an in-season irrigation management tool—without greatly increasing the data input requirement compared to YieldTracker.

CONCLUSIONS

YieldTracker offers a straightforward way to predict grain yields of graminoid crops to guide water application decisions with minimal input of crop and weather data under irrigated conditions. Crop inputs are limited to one or more estimates of LAI to calibrate the seasonal course of canopy development. Remote sensing offers an affordable way to project LAI on a wide-area basis, but requires a vegetation index that is sensitive to LAI values as high as 6. Total chlorophyll index, or SR in a narrow band within the red edge spectral region, both appear to satisfy this requirement. A water band index may allow modulation of biomass production and allocation algorithms to prevent overprediction of productivity during periods of water stress. Nevertheless, it may be more fruitful to account for water deficit effects using a water balance approach.

ACKNOWLEDGMENTS

This research was funded by the Kansas Agricultural Experiment Station and the Ogallala Aquifer Program, a consortium among USDA–Agricultural Research Service, Kansas State University, Texas AgriLife Research, Texas AgriLife Extension Service, Texas Tech University, and West Texas A&M University.

REFERENCES

- Bastiaanssen, W.G.M., M. Menenti, R.A. Feddes, and A.A. Holtslang. 1998. A remote sensing surface energy balance algorithm for land (SEBAL): I. Formulation. *J. Hydrol.* 212–213:198–212.
- Earl, H.J., and R.F. Davis. 2003. Effect of drought stress on leaf and whole canopy radiation use efficiency and yield of maize. *Agron. J.* 95:688–696.
- Elvidge, C.D., and Z. Chen. 1995. Comparison of broad-band and narrow-band red and near-infrared vegetation indices. *Remote Sens. Environ.* 54:38–48.
- Gamon, J.A., H.-L. Qiu, D.A. Roberts, S.L. Ustin, D.A. Fuentes, A. Rahman, D. Sims, and C. Styliniski. 1999. Water expressions from hyperspectral reflectance: Implications for ecosystem flux modeling. *In* R.O. Green (ed.) *Summaries of the Eighth JPL Airborne Earth Science Workshop*. 9–11 Feb. 1999. Jet Propulsion Laboratory, Pasadena, CA.
- Gitelson, A.A., Y. Gritz, and M.N. Merzlyak. 2003. Relationships between leaf chlorophyll content and spectral reflectance and algorithms for non-destructive chlorophyll assessment in higher plant leaves. *J. Plant Physiol.* 160:271–282.
- Ko, J., S.J. Maas, R.J. Lascano, and D. Wanjura. 2005. Modification of the GRAMI model for cotton. *Agron. J.* 97:1374–1379.
- Maas, S.J. 1988a. Use of remotely-sensed information in agricultural crop growth models. *Ecol. Modell.* 41:247–268.
- Maas, S.J. 1988b. Using satellite data to improve model estimates of crop yield. *Agron. J.* 80:655–662.
- Maas, S.J. 1992. GRAMI: A crop growth model that can use remotely sensed information. ARS-91. USDA-ARS, Washington, DC.
- Maas, S.J. 1993. Parameterized model of graminaceous crop growth: II. Within-season simulation calibration. *Agron. J.* 85:354–358.
- Maas, S.J., R.J. Lascano, and D.E. Cooke. 2003. Web-based yield prediction information delivery system. p. 35–36. *In* Proc. Integrated Biological Systems Conf., San Antonio, TX. Available at http://beaumont.tamu.edu/conference/BioSystem2003_Booklet.pdf (verified 20 Feb. 2009).
- Mutanga, O., and A.K. Skidmore. 2004. Narrow band vegetation indices overcome the saturation problem in biomass estimation. *Int. J. Remote Sens.* 25:3999–4014.
- Myneni, R.B., R.R. Nemani, and S.W. Running. 1997. Estimation of global leaf area index and absorbed PAR using radiative transfer models. *IEEE Trans. Geosci. Rem. Sens.* 35:1380–1393.
- Peñuelas, J., I. Filella, C. Biel, L. Serrano, and R. Savé. 1993. The reflectance at the 950–970 nm region as an indicator of plant water status. *Int. J. Remote Sens.* 14:1887–1905.
- Serrano, L., I. Filella, and J. Peñuelas. 2000. Remote sensing of biomass and yield of winter wheat under different nitrogen supplies. *Crop Sci.* 40:723–731.
- Sinclair, T.S. 1991. Canopy carbon assimilation and crop radiation-use efficiency dependence on leaf nitrogen content. p. 95–107. *In* K.J. Boote and R.S. Loomis (ed.) *Modeling Crop Photosynthesis—from Biochemistry to Canopy*. CSSA Spec. Publ. 19. CSSA, Madison, WI.
- Welles, J.M., and J.M. Norman. 1991. Instrument for indirect measurement of canopy architecture. *Agron. J.* 83:818–825.